UV Raman Spectroscopic Study on TiO_2. II. Effect of Nanoparticle Size on the Outer/Inner Phase Transformations

Jing Zhang,[†,§] Qian Xu,[†,‡,§] Meijun Li,[†] Zhaochi Feng,[†] and Can Li*[,†]

State Key Laboratory of Catalysis, Dalian Institute of Chemical Physics, Chinese Academy of Sciences, P.O. Box 110, Dalian 116023, China, and Graduate University of Chinese Academy of Sciences, Beijing 100049, China

Received: September 09, 2008; Revised Manuscript Received: November 19, 2008

The mechanism of the size-dependent outer/inner phase transformation in ultrafine TiO_2 particles with narrowed size distribution was intensively investigated using UV Raman spectroscopy, X-ray diffraction, and transmission electron microscopy. Particle size is found to be the critical parameter determining the onset transition temperature and nucleation performance. The transformation temperature was decreased with the decrease of initial particle size. Rutile nucleates at interfaces of the contacting anatase grains ($<$60 nm). The free surface, interface, and bulk are all likely to work as rutile nucleation sites for large particles($\geq$60 nm). Thermal stability of nanoscale titania is significantly enhanced by the presence of La_2O_3 even with surface coverage less than 5%, which blocks the outer/inner phase transformation of nano anatase. A model was devised to describe the phase transformation as a function of particle size and to predict the phase stability.

1. Introduction

Titanium dioxide (TiO_2) is among the most extensively studied materials for its various properties and applications in conventional catalyst support,[1] pigment,[2] photocatalysis,[3,4] solar cells,[5−8] and sensing.[9−11] Nanocrystallinine titania has recently attracted considerable attention as a result of the advanced size-dependent chemical and physical properties, such as quanta effect, surface effect, regional confinement of matter, and high surface areas, etc. The phase structure and particle size have been found to be critical parameters in determining their suitability for practical applications.[12,13]

Among the crystalline forms of TiO_2, anatase and rutile are the two most common polymorphs. The different structures of the two phases exhibit different physical properties, leading to different applications. For instance, anatase is commonly employed as catalyst support and photoelectrochemical material for its chemical and optical activity, while rutile is largely used in pigments for its effective light scattering. Therefore, understanding the mechanism of phase transformation and controllable tuning phase composition is important for the application of TiO_2, particularly in photocatalysis.

Thermodynamically, the rutile phase is stable and anatase is metastable at ambient pressure and temperature.[14] Thermodynamics indicates that phase stability is dependent on the particle size and it is found that anatase is more stable than rutile with decreasing the particle size to nanometer scale.[15,16] On the basis of the inferred lower surface energy of nancrystalline anatase, Banfield et al. have reported that particle size significantly affects the transformation rate for nanocrystalline TiO_2.[15,17] Thus, a grand challenging question requires addressing: what is the effect of particle size on the mechanism of phase transformation, especially the phase transformation behavior in nanoparticles?

Upon light capture the excited charge carriers (electrons and holes) of TiO_2 as a promising photocatalyst are highly reactive radicals with robust reductive and oxidative capacity, respectively, that may recombine, nonradiatively or radiatively (dissipating the input energy as heat), get trapped, and react with electron donors or acceptors adsorbed on the photocatalyst surface. The current studies have demonstrated that mixed-phase of TiO_2 typically displayed higher photoactivity than the pure phase.[18−21] The enhanced activity is regarded as the synergistic effect between anatase and rutile, which favors the spatial separation of photogenerated charge carriers. Our latest discoveries[22] reveal that the surface-phase junction between anatase and rutile more rather contributes directly to photocatalysis, suggesting the importance of tuning the surface phase structure. UV Raman spectroscopy is one of the most powerful surface-sensitive techniques for the strong-absorption at ultraviolet samples,[23] making it particularly useful to investigate the temperature-induced surface phase structural transitions that occur in TiO_2.

We have previously demonstrated that the phase transformation of agglomerated TiO_2 particles with diameters in the range of 15−40 nm starts from the interfaces of the contacting anatase grains and that phase transformation in the outer region is not in the same step as that in the inner region.[23] This raises another question whether such mechanism would be general for TiO_2 with a wide range of particle sizes? The strategy of this work is to investigate the effect of particle size on the outer/inner phase transformation by preparing TiO_2 spheres with ultrafine and narrow size distribution. Herein, we prepared TiO_2 particles with average diameter from nanometer scale to submicrometere scale (7−300 nm). The crystalline phases were determined by a surface sensitive technique, UV Raman spectroscopy combined with X-ray diffraction (XRD) and transmission electron microscopy (TEM). Compared to inner phase transformation,

* To whom correspondence should be addressed. Telephone: +86-411-84379070. Fax: +86-411-84694447. E-mail: canli@dicp.ac.cn
† Dalian Institute of Chemical Physics, Chinese Academy of Sciences.
‡ Graduate University of Chinese Academy of Sciences.
§ These authors contributed equally to this work.

10.1021/jp808013k CCC: $40.75
Published on Web 01/09/2009

an obvious hysteresis occurs for outer phase transformation in the nano scale. It is notable that the interface nucleation governs the phase transformation of nanoparticles, while the transition in larger particles (≥60 nm) is dominated by the accumulation of interface, free surface, and bulk nucleation. Moreover, the controllable phase was achieved by a simple method involving impregnating a small amount of La_2O_3 and subsequent calcinating at high temperatures.

2. Experimental Section

Synthesis of the Fairly Uniform Anatase TiO_2 Nanoparticles (7−25 nm, denoted as A7, A10, A15, and A25). The preparation procedure of TiO_2 nanoparticles was analogous to the gel−sol method described previously.[31] In a typical synthesis, a 9-mL triethanolamine (TEOA: $N(CH_2CH_2OH)_3$) solution was mixed with a amount of Lutensol TO7 (i-$C_{13}H_{27}O(CH_2CH_2O)_7H$), followed by addition of 10 mL of titanium isopropoxide at ambient temperature. Doubly distilled water was added to the mixed solution in order to obtain a Ti^{4+} ion concentration of 0.50 mol dm^{-3}. The solution was adjusted to 0.9, 2.8, 4.2, and 7.8 by adding nitric acid, respectively. The final solution was transferred to a Teflon-lined autoclave and aged at 100 °C for 24 h and then aged at 140 °C for 72 h. The solid was collected after centrifuging the suspension. The precipitate was washed with doubly distilled water, and was vacuum-dried at 60 °C for 24 h.

Synthesis of the Fairly Uniform Anatase TiO_2 Nanoparticles (60 nm, denoted as A60). Titanium tetrachloride ($TiCl_4$) was used as the precursor. It was added slowly into ice water under stirring to prepare a 0.2 mol/L $TiCl_4$ solution. This solution was slowly dropped into the mixture of deionized water, $NH_3 \cdot H_2O$, and CTMAB under vigorous stirring at room temperature until the pH value of the solution reached ~8. The concentration of CTMAB in the solution is in the critical micelle concentration. The produced white precipitate was filtered and washed with distilled water until chloride ions were not detectable in the washed water, and the solid sample was then dried at 120 °C for 12 h.

Synthesis of the Sub-Micrometered Anatase TiO_2 Spheres (300 nm, denoted as A300). TiO_2 spheres (300 nm) were prepared based on sol−gel processing via a controlled colloidal process described by Keshmiri et al. Titanium tetraisopropoxide ($Ti(OPr)_4$) was added dropwise to mixed anhydrous ethyl alcohol and TO_7 solution, followed by addition of doubly distilled deionized water. According to preparation method described by Keshmiri et al., the addition of doubly distilled deionized water to the mixed solution was took place in two steps, a part (10 wt %) before introducing $Ti(OPr)_4$ to the solution and the other part 10 min after that. The molar ratio of the water/$Ti(OPr)_4$ was controlled to be 190. The solution was strongly stirred for 30 min at ambient temperature and then aged for 20 h. The produced suspensions were centrifuged and washed with distilled water and then were dried in a vacuum oven at 60 °C for 24 h.

Synthesis of La_2O_3-Covered TiO_2 (La_2O_3/TiO_2). The A10, A15, and A25 sample calcined at 500, 700, and 800 °C, respectively, was used as a support. La_2O_3/A10, La_2O_3/A15, and La_2O_3/A25 samples, containing different amounts of La_2O_3 (0.1−3 wt %), were prepared by a wet impregnation method,[23] and then calcined at 660, 860, and 980 °C, respectively. A10, A15, and A25 samples were calcined at 660, 860, and 980 °C, respectively for comparison with the La_2O_3/A10, La_2O_3/A15, and La_2O_3/A25 samples.

All these samples were calcined at a relevant temperature in air for 4 h.

Characterization. UV Raman spectra were measured at room temperature on a self-assembled UV Raman spectrograph with a Jobin-Yvon T64000 triple-stage spectrograph with the spectral resolution of 2 cm^{-1}. The laser line at 325 nm of a He−Cd laser was used as an exciting source with an output of 25 mW. The power of laser at sample was about 3.0 mw. XRD patterns were obtained on a Rigaku MiniFlex diffractometer with Cu Kα radiation source. Diffraction patterns were collected from 20−80° at a speed of 5°/min. TEM images were obtained using a JEM-2000 EX apparatus operating at 100 kV.

3. Results and Discussion

The Morphology and the Initial Particle Size of the As-Prepared Samples. Figure 1 displays the TEM micrographs of the as-prepared TiO_2 samples, exhibiting uniform spherical geometry with the average diameters of c.a. 7, 15, 25, 60, and 300 nm (denoted as A7, A15, A25, A60, and A300), respectively. The corresponding results from XRD patterns and UV Raman spectra (not shown) suggest that the samples prepared are all in the anatase phase.

Outer/Inner Phase Transformation of As-Prepared Samples with Different Initial Particle Sizes. As illustrated in Figure 2a, the inner phase transformation occurs at about 360 °C as evidenced by the appearance of the weak peaks (2θ = 27.6, 36.1, 41.2, and 54.3°) due to rutile phase, whose content in the bulk of A7 sample is estimated to be 16.3 wt %. The content of rutile is increased respectively to 44.6 and 72.5 wt % when the calcination temperatures were correspondingly increased to 400 and 500 °C. The inner region of the A7 sample is almost in the rutile phase (94 wt %) after a calcination at 600 °C. The changes of the outer crystalline phase and phase composition during the phase transformation of A7 sample are monitored by UV Raman spectroscopy (Figure 2b). UV Raman spectrum of the A7 sample calcined at 400 and 500 °C indicates that the mixed phases of anatase and rutile coexist in the outer region, and the rutile content is about 47 and 64 wt %, respectively. Obviously, the rutile content estimated by UV Raman spectra (Figure 2b) is almost coincident with that estimated by XRD patterns (Figure 2a), indicating that the phase transformation in the outer region nearly keeps in the same step as that in the inner region for A7 sample.

The phase transition of the A7 sample was further investigated by TEM (Figure 3). Compared to the as-prepared sample (Figure 1a), the morphology and particle size were basically preserved after calcination at 300 °C (Figure 3a), although particles become agglomerated. In contrast, the particle size increases obviously (Figure 3b) when the temperature is increased to 400 °C, e.g., TiO_2 particles with 30 nm were observed. As shown in Figure 2a, the phase transformation takes place at about 360 °C. These results imply that the phase transformation is accompanied by a rapid grain growth, i.e., the phase transformation from anatase to rutile can significantly enhance the grain growth.[24] Moreover, it is observed that the agglomeration of the TiO_2 particles occurs along with the anatase-to-rutile phase transformation.

Figure 4b gives the rutile contents in the inner and outer region of the A15 sample (circle) with increasing the calcination temperature (XRD patterns and UV Raman spectra of the A15 sample calcined at different temperatures are supplied as the Supporting Information). It is found that the A15 sample starts to transform into the rutile phase at 735 °C in the inner region. The content of the rutile phase in the bulk is 13.3 wt % for the A15 samples calcined at 750 °C. The UV Raman spectra indicate that the outer region

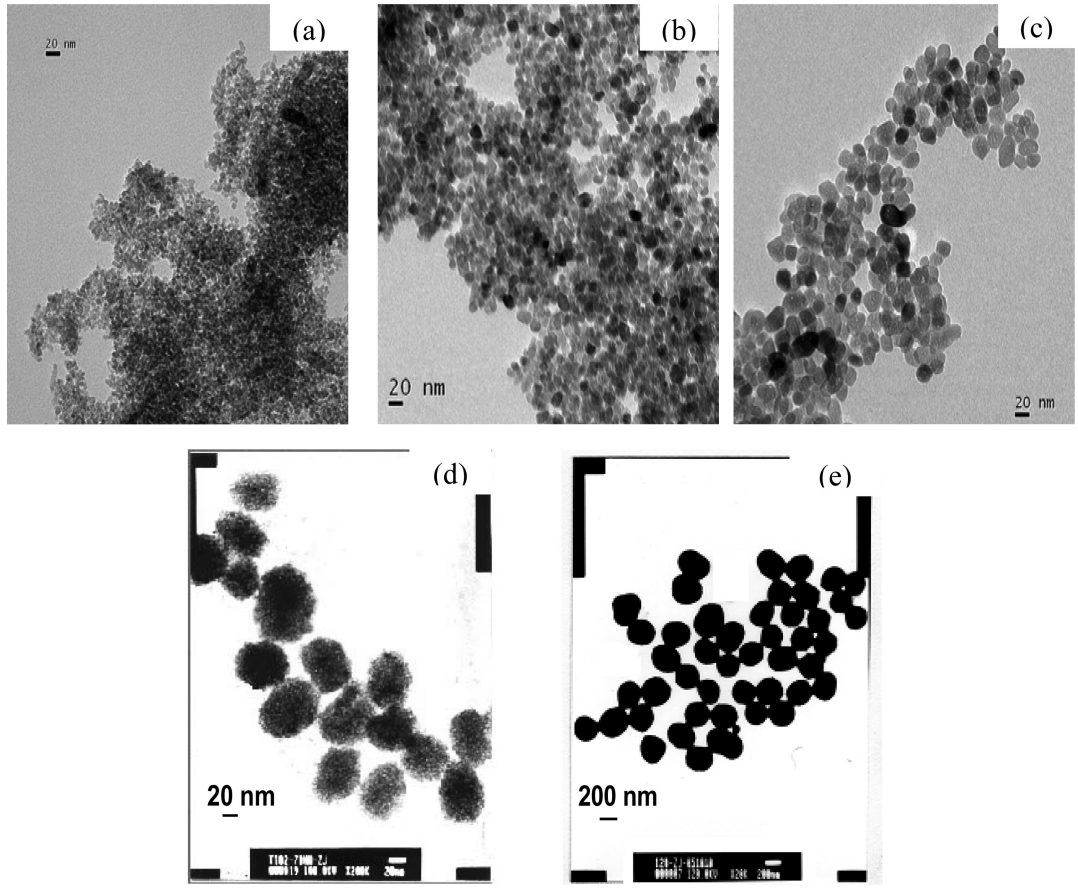

Figure 1. TEM micrographs of the as-prepared ultrafine TiO_2 samples with narrowed size distribution.

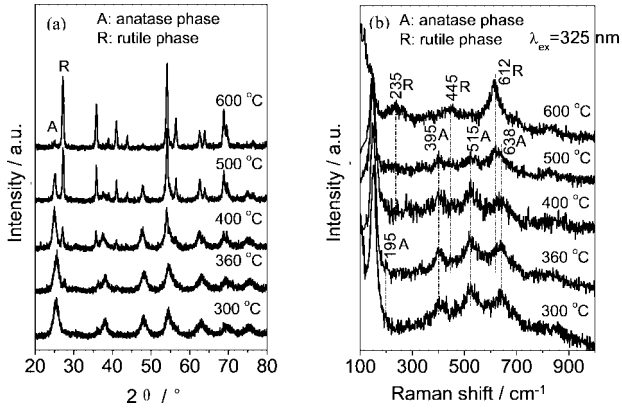

Figure 2. (a) XRD patterns and (b) UV Raman spectra of 7 nm TiO_2 particles calcined at different temperatures.

is still in the pure anatase phase for the A15 sample, while the inner region contains up to 80 wt % rutile phase for the sample calcined at 800 °C. When the calcination temperature is further increased to 850 °C, the rutile content in the inner and outer region is about 90 and 40 wt %, respectively. After a calcination at 860 °C, the anatase phase completely transforms into the rutile phase. Obviously, there is great difference between the outer and inner phase composition for the A15 sample. This suggests that phase transformations in the outer region and in the inner are in very different step under calcination. The phenomena that the outer phase is different from the inner phase during the phase transformation are also observed for the A25 sample (triangle) shown in Figure 4b, which is also consistent with our previous results.[23] In combination with the results of the A7 sample, we would draw a conclusion that the mechanism of phase transformation for the sample with the particle size <10 nm is quite different from that for the sample with the particle size exceeding 10 nm.

However, it is of interest that the crystalline phase and phase composition in the outer are very similar to that in the inner for the A60 (star) and A300 (diamond) samples during the phase transformation (Figure 4c). Namely, the phase transformation rates in the outer region and in the inner are quite close under calcination. For example, after calcination at 980 °C, the rutile contents in the bulk and in the surface are 96 and 73 wt % for the A60, respectively. It is observed that the grain growth process could be significantly enhanced with the phase transformation from anatase to rutile for the A60 and A300 samples (TEM images of A60 sample calcined at different temperatures are supplied as the Supporting Information).

The Outer/Inner Onset Transition Temperature and the Hysteresis of Outer Phase Transformation. The results from Figure 5 were used to estimate the onset of phase transformation as a function of particle size. It is obvious that the onset of phase transformation is shifted to lower temperatures when the particle size decreases (Figure 5a). It is generally agreed that the solid−solid phase transformation nucleates at defects. Defects can be annealed out more easily in nanoparticles than in extended solids, because the distance defects would travel to reach the surface in nanoparticles is much smaller and the temperature required for annealing is lower.[25]

More specifically, by plotting the onset temperature (T_{inner} and T_{outer} for inner and outer onset temperature, respectively) of phase transformation vs initial particle size (d, nm), a very good fit was obtained using the following expressions

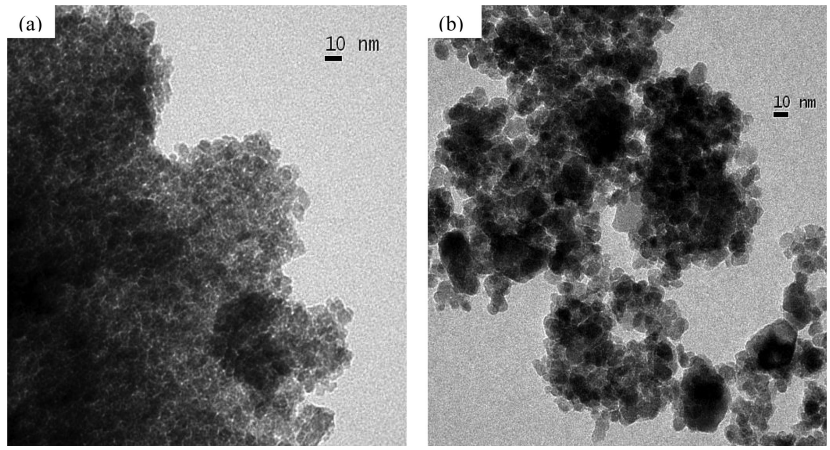

Figure 3. TEM micrographs of 7-nm TiO_2 partilces calcined at (a) 300 and (b) 400 °C.

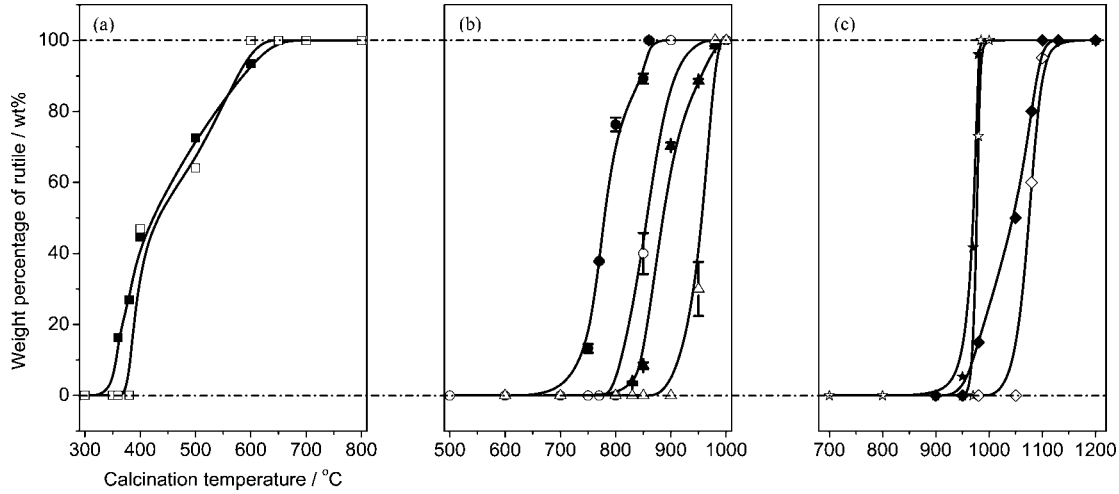

Figure 4. Weight percentage of rutile in the inner (solid) and outer (open) region of TiO_2 samples with the particle sizes of (a) 7 nm (square), (b) 15 nm (circle) and 25 nm (triangle), and (c) 60 nm (star) and 300 nm (diamond) estimated by XRD and UV Raman spectroscopy.

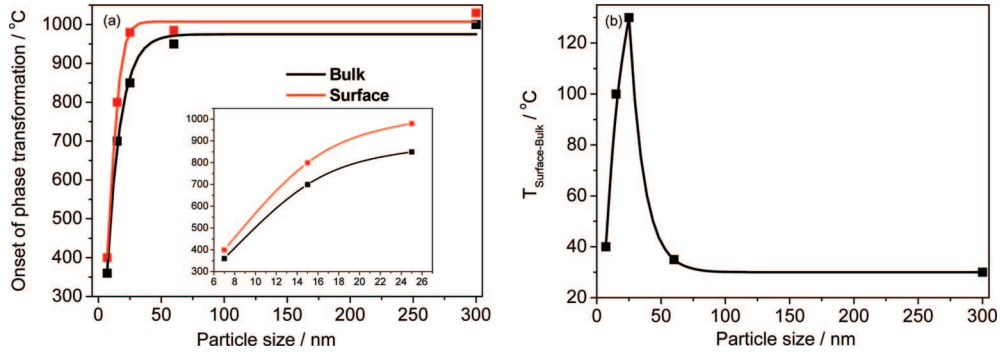

Figure 5. (a) Plot of the onset temperature of phase transformation versus initial particle size. (b) Plot of temperature difference between outer and inner onset temperature of phase transformation versus initial particle size. Curves are fitted based on experimental data.

$$T_{\text{inner}}(\text{K}) = 1248.5 - 1180.3\ \exp(-0.09388d)(R^2 = 0.99471) \quad (1)$$

$$T_{\text{outer}}(\text{K}) = 1285.7 - 1620.3\ \exp(-0.1385d)(R^2 = 0.99459) \quad (2)$$

The above functions are assumed appropriate in approximating the real case. As described in the expressions, the outer onset temperature (T_{outer}) is higher than the inner one (T_{inner}), indicating that the outer transition lags behind the inner transition for the agglomerated titania particles in general. It is required a certain temperature and/or time for the propagation of phase transformation from the inner to the outer, which depends on the initial particle size.

The function of T_{inner} and T_{outer} tends to level off when the particle sizes are quite large ($d \rightarrow \infty$). It follows that the outer transformation occurs when the inner phase transformation of the extended solid happens. As the particles grow sizable, the phase transformation then proceeds by complex kinetics involving multiple nucleation and domain fracture,[26] which makes the phase transitions occur at quite a high temperature. At such high temperatures, thermal fluctuation of Ti and O atoms in anatase is considerably strong, and the rutile phase emerges on the outer of coarse particles as soon as the inner phase transformation

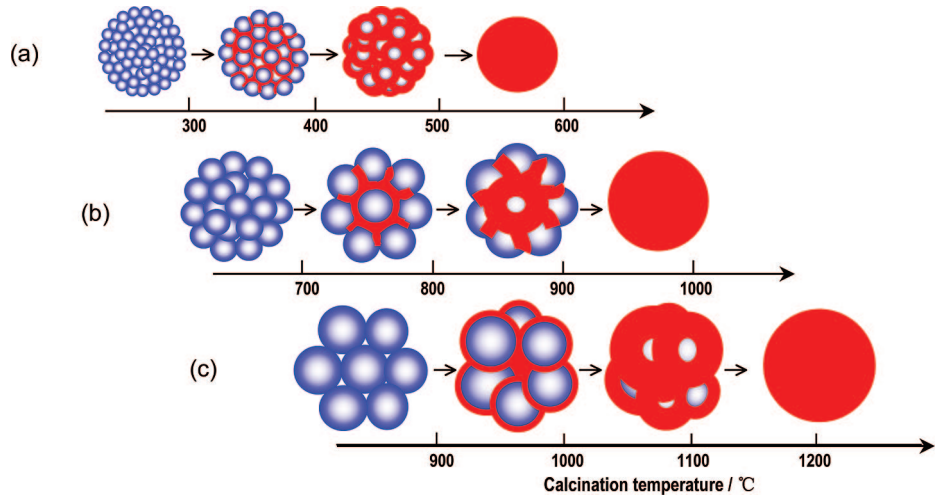

Figure 6. A proposed scheme for the phase transformation of TiO_2 with the particle size (a) smaller than 10 nm, (b) in the range of 10−60 nm, and (c) larger than 60 nm.

occurs. The phase transformations of A60 and A300 samples start at 950 and 980 °C, respectively, acting in accordance with the phenomena of the extended solid, and in consequence they can be ideally considered as extended solid.

Roughly, the variation can be considered linear for smaller particles [eqs 1 and 2 at $d \rightarrow 0$], and the slope of T_{outer} function is larger than that of T_{inner} function, which can be interpreted as that the temperature difference in outer and inner onset becomes progressively distinct with the increase of particle size within a certain range. However, functions T_{outer} and T_{inner} for the TiO_2 nanoparticles (A7, A15, and A25 samples) with particle sizes between the two extreme cases almost follow parabolic curve. Inserted in Figure 5a is the enlarged section of the transition onset temperature for TiO_2 particles ranging from 7 to 30 nm. It is noteworthy that the hysteresis of outer transition is more distinct for nanoparticles. A more direct comparison of the difference between outer and inner onset temperature of phase transformation described in Figure 5b reveals another interesting result: the effect of particle size upon the difference is readily apparent, i.e., the difference is sharper for nanoparticles, and the maximum is found for A25 (25 nm, TiO_2). Since the particle size is larger, the greater distance the propagation of phase transformation must travel if inner phase transformation of agglomerated particles occurs, and thus, the slower rate of phase transformation in outer is observed. On the other hand, it is expected that the onset temperature of phase transformation required for larger particles is higher than that for smaller ones. Accordingly, very high temperature would provide enough energy to complete the phase transformation of the whole particle quickly. By consideration of those two factors, it is not difficult to understand the presence of maximum temperature difference. Moreover, on the basis of the above analysis, the phase transformation of nanoparticles is more sensitive to the temperature compared to extended solids. For this reason, maximum temperature difference occurs in nanoparticles is necessary, say, 25 nm obtained in our experiment.

The Proposed Mechanism of Size-Dependent Phase Transformation and Thermal Stability of Titania Nanoparticles in the Presence of La_2O_3. These results clearly demonstrate that the mechanism of the phase transformation in TiO_2 particles depends strongly on the particle size. A proposed scheme for the phase transformation of TiO_2 with different particle sizes is illustrated in Figure 6. It should be noted that the proposed model is based on the agglomerated TiO_2 particles. The phase transformations take place at lower temperatures for smaller particles (<10 nm). Thermodynamically, the surface energy of nanocrystalline materials is very high for their large specific surface areas. The thermodynamic driving force of phase transformation may come mainly from the high surface energy, and it will increase dramatically with the decrease of particle size. This means that the smaller the particle size is the lower the potential barrier of reaction is and consequently the easier the phase transformation occurs. Thermal fluctuation of Ti and O atoms in anatase is not strong enough to generate rutile nuclei on the surfaces or in the bulk of a grain at lower temperatures.[27] However, at a subset of anatase interfaces, structural elements with rutile-like character can be produced,[28] and they may serve as rutile nucleation sites. The solid-phase transformation is a process of nucleation and growth. On the other hand, Zhang et al.[17] have stated that the formation of a rutile particle happens simultaneously with the nuclei growth and involves growth at the particle−particle neck from constituents evidently provided by surface diffusion. Since the low transition onset temperature can reduce the collision frequency of the particles, the nucleation rate is low, and the rate of rutile nucleation becomes the rate-determining step of phase transformation and the nuclei growth can be considered instantaneous. Therefore, once the nucleation is initiated at the interfaces between the contacted anatase particles, the phase transformation can quickly spread through the whole agglomerated particles. Thus, it is difficult to differentiate phase transformation in the outer from that in the inner, that is, the outer and inner phase transformation almost proceed simultaneously (see Figure 4a).

When the TiO_2 particle size is in the range of 10−60 nm, the rutile phase nucleates at intermediate temperatures. Zhang et al.[27,30] indicated that the activation energy for interface nucleation increases with decrease in particle size. Therefore, the interface nucleation still dominates the phase transformation of nanoparticles with the size in the range of 10−60 nm. The particle size of the TiO_2 sample prepared by conventional methods, such as sol−gel and precipitation method, is normally in the range of 10−60 nm. We have previously indicated that the outer crystalline phases of TiO_2 with the initial particle size ranging from 15−40 nm are different from inner crystalline phases during the phase transition.[23] In this work, we carried out the systematic investigation of the particle size effect on the outer/inner phase transformation by preparing ultrafine particles with narrowed size distribution. We are more concerned

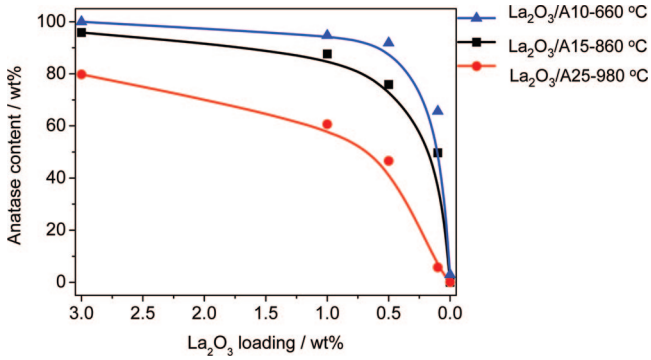

Figure 7. Weight percentage of anatase in La_2O_3/A10, La_2O_3/A15, and La_2O_3/A25 vs the loading of La_2O_3.

about the outer properties and the outer/inner quantitative analysis of phase composition. For an anatase sample with a unit volume, the smaller the initial particle size (D_0), the larger the concentration of interface nucleation sites (N_a).[30] In addition, since the rate of interface nucleation is proportional to N_a,[27] the larger the nanoparticles, the lower the nucleation rate. Thus, more additional time is needed for the nuclei to grow to the entire volume with simultaneous growth of the rutile particle. Therefore, from macroscopic view, the outer phase transformation lags behind the inner phase transformation and the trend of hysteresis is more obvious with the increase of the initial particle size in a certain range (illustrated in Figures 4 and 5).

As discussed above, the rutile phase nucleates mainly at the interfaces of contacting anatase grains when the particle size is smaller than 60 nm; thus, if the nucleation sites are inactive, the phase transformation should be retarded or prohibited. Our previous work[23] indicated that La_2O_3 would be a perfect stabilizer of the anatase phase. Therefore, we impregnated the A10, A15, and A25 samples with highly dispersed La_2O_3 (see Experimental section, the corresponding sample was denoted as La_2O_3/A10, La_2O_3/A15, and La_2O_3/A25) and then calcined at the designated temperatures, respectively. (The selected calcination temperature was 660, 860, and 980 °C for La_2O_3/A10, La_2O_3/A15, and La_2O_3/A25 samples. The A10, A15, and A25 samples without La_2O_3 can be transformed into the rutile phase at the corresponding calcination temperatures.)

Figure 7 shows the inner anatase content for the La_2O_3/A10, La_2O_3/A15, and La_2O_3/A25 samples vs the loading of La_2O_3 (corresponding XRD patterns are supplied as Supporting Information). It is very interesting to note that the impregnation of only 0.5 wt % La_2O_3 can obviously stabilize the anatase phase in the inner of A10 sample calcined at 660 °C (denoted as La_2O_3/A10−660 °C), while A10 sample completely transforms to rutile phase at about 660 °C. For the La_2O_3/A15 sample, the anatase phase can be maintained after a calcination even at 860 °C when the loading of La_2O_3 is 1 wt %. For the La_2O_3/A25 sample, impregnation of 3 wt% La_2O_3 can stabilize the anatase phase even up to 980 °C. These interesting results clearly demonstrate that the anatase phase of TiO_2 nanoparticles can be stabilized at higher temperature even with low surface loading of La_2O_3 and further confirm the aforementioned mechanism of the phase transformation.

The results of UV Raman spectra (not shown) of the La_2O_3/A10 sample calcined at 660 °C and La_2O_3/A15 sample calcined at 860 °C indicate the outer region of these samples is stabilized in the anatase phase when La_2O_3 loading is only 0.1 wt %. For the La_2O_3/A25 sample, the impregnation of 0.5 wt % La_2O_3 can stabilize the outer anatase phase after calcination at 980 °C. These results suggest that not only the anatase−rutile phase transformation is significantly retarded but also the further propagation of the rutile phase into the outer of agglomerated particles is slowed remarkably by surface modification of La_2O_3.

Regarding the stabilization mechanism, a detailed analysis of surface properties should be taken into account. Since La_2O_3 could not be detected in XRD nor UV Raman spectra, the lanthanum species should be dispersed highly onto the surface of the anatase particles. It can be seen that in our experiment the surface loading of La_2O_3 is far lower than monolayer coverage and that the separation of anatase clusters may be incomplete, while the phase transformation can still be retarded or prohibited, suggesting that nucleation sites are not located in the whole surface of the single anatase grain but in the particular region of anantase surface. Generally, the defect sites on the surface of the anatase grains are assumed to play an important role in the phase transformation of TiO_2. The anatase grains containing a higher defect density tend to coalesce by reaction of their respective surface defects. The surface-dispersed La_2O_3 possibly react with the defect sites or make them inactive, correspondingly reducing the defect concentration and surface energy, thus inhibiting the reaction between nanoparticles. As a consequence, the anatase phase is stabilized.

For smaller anatase particles, the transformation temperature is relatively lower and the interface nucleation is the main nucleation mode. Once the defect concentration is reduced, the phase transformation can be inhibited. Therefore, the stabilization effect of La_2O_3 on anatase TiO_2 is more distinct in La_2O_3/A10 sample than the others. Since the calcination temperatures of La_2O_3/A15 and La_2O_3/A25 samples are relatively higher, the free surface of the anatase particle at high temperatures can also serve as nucleation site, although the interface nucleation still governs nucleation. As a result, the relatively higher content of highly dispersed La_2O_3 is needed not only for occupying the defect sites but also for covering the surfaces of the anatase particles to stabilize the anatase.

As the predicted dependence of the grain−grain contact number N_a on the initial particle size is $1/D_0^3$;[30] thereby we can infer that the proportion of interface nucleation in larger TiO_2 ($\geq$60 nm) would be smaller with respect to the nanopartilces. At a solid surface, the coordination numbers are less than those in the bulk; thus more chemical bonds have to be broken in the bulk nucleation. Accordingly, the activation energy for bulk nucleation is greater than that for surface and interface nucleation, and thus relatively high temperature is required for phase transformation. Such a strong thermal fluctuation can provide sufficient energy to overcome the potential barrier of surface, interface, and even bulk nucleation. The formation of multiple nuclei in terms of a single anatase crystal particle causes the transformation to proceed throughout the whole particle quickly. As a result, it is observed that the outer phase transformation nearly keeps the same rate as the inner phase transformation.

The systematic investigation of outer/inner phase transformation demonstrates a strong particle-size dependence of nucleation mechanism. Figure 8 shows the activation energy-related function. It is observed that the plots (see the inserted section) of the nanoparticles ($<$60 nm) are of very good linearity and the slope is smaller than that of larger particles ($\geq$60 nm), which further illustrates that the nanoparticles follow the similar nucleation and that the active energy of bulk nucleation is greater than that of interface nucleation.

4. Conclusions

In summary, we have demonstrated that the hysteresis of outer phase transformation is common for the phase transformation

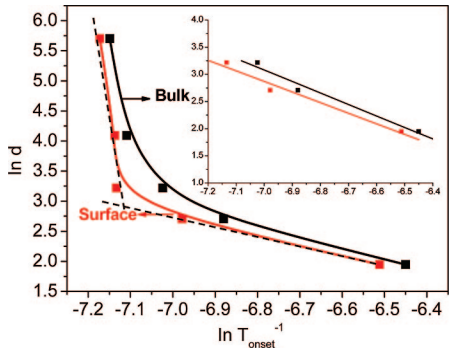

Figure 8. The natural logarithm transformation of initial particle size (d, nm) vs the natural logarithm transformation of $1/T_{onset}$ (K^{-1}).

of nanoparticles and that interface/bulk nucleation mechanism can be reasonably employed to interpret the distinct phenomena during phase transformation for TiO_2 with different particle sizes. Experimentally, an exponential expression is fitted to relate the onset temperature of outer/inner phase transformation with initial particle size. Our proposed nucleation mechanism is consequently confirmed on the basis of relationship between outer/inner phase transformation and particle size. Furthermore, the efficient control of the crystalline phase of TiO_2 by a simple surface modification would have promising applications in solar cell and photocatalysis.

Acknowledgment. This work is financially supported by National Basic Research Program of China (Grant No. 2003CB214504), Programme Strategic Scientific Alliances between China and The Netherlands (Grant No. 2008DFB50130), the Knowledge Innovation Program of the Chinese Academy of Sciences (Grant No. DICP K2006E2), and National Natural Science Foundation of China (NSFC Grant No. 20673112). We thank Dr. Wenhua Zhang for discussions.

Supporting Information Available: XRD patterns and UV Raman spectra of A15 calcined at different temperatures, TEM images of A60 calcined at 800, 950, and 1000 °C, and XRD patterns of La_2O_3/A10, La_2O_3/A15, and La_2O_3/A25 samples with increasing La_2O_3 loading. This material is available free of charge via the Internet at http://pubs.acs.org.

References and Notes

(1) Bradford, M. C. J.; Vannice, M. A. *Appl. Catal. A: Gen.* **1996**, *142*, 73.
(2) Pfaff, G.; Reynders, P. *Chem. Rev.* **1999**, *99*, 1963.
(3) Linsebigler, A. L.; Lu, G. Q.; Yates, J. T. *Chem. Rev.* **1995**, *95*, 735.
(4) Thompson, T. L.; Yates, J. T. *Chem. Rev.* **2006**, *106*, 4428.
(5) Bach, U.; Lupo, D.; Comte, P.; Moser, J. E.; Weissortel, F.; Salbeck, J.; Spreitzer, H.; Grätzel, M. *Nature* **1998**, *395*, 583.
(6) Oregan, B.; Grätzel, M. *Nature* **1991**, *353*, 737.
(7) Grätzel, M. *J. Photochem. Photobiol. C* **2003**, *4*, 145.
(8) Grätzel, M. *Nature* **2001**, *414*, 338.
(9) Paulose, M.; Varghese, O. K.; Mor, G. K.; Grimes, C. A.; Ong, K. G. *Nanotechnology* **2006**, *17*, 398.
(10) Varghese, O. K.; Mor, G. K.; Grimes, C. A.; Paulose, M.; Mukherjee, N. *J. Nanosci. Nanotechnol.* **2004**, *4*, 733.
(11) Mor, G. K.; Carvalho, M. A.; Varghese, O. K.; Pishko, M. V.; Grimes, C. A. *J. Mater. Res.* **2004**, *19*, 628.
(12) Zhang, Z. B.; Wang, C. C.; Zakaria, R.; Ying, J. Y. *J. Phys. Chem. B* **1998**, *102*, 10871.
(13) Carp, O.; Huisman, C. L.; Reller, A. *Prog. Solid State Chem.* **2004**, *32*, 33.
(14) Shannon, R. D.; Pask, J. A. *J. Am. Ceram. Soc.* **1965**, *48*, 391.
(15) Gribb, A. A.; Banfield, J. F. *Am. Mineral.* **1997**, *82*, 717.
(16) Zhang, H. Z.; Banfield, J. F. *J. Mater. Chem.* **1998**, *8*, 2073.
(17) Zhang, H. Z.; Banfield, J. F. *Am. Mineral.* **1999**, *84*, 528.
(18) Jiang, D. L.; Zhang, S. Q.; Zhao, H. J. *Environ. Sci. Technol.* **2007**, *41*, 303.
(19) Sung, Y. M.; Lee, J. K.; Chae, W. S. *Cryst. Growth Des.* **2006**, *6*, 805.
(20) Kawahara, T.; Ozawa, T.; Iwasaki, M.; Tada, H.; Ito, S. *J. Colloid Interface Sci.* **2003**, *267*, 377.
(21) Yan, M. C.; Chen, F.; Zhang, J. L.; Anpo, M. *J. Phys. Chem. B* **2005**, *109*, 8673.
(22) Zhang, J.; Xu, Q.; Feng, Z. C.; Li, M. J.; Li, C. *Angew. Chem., Int. Ed.* **2008**, *47*, 1766.
(23) Zhang, J.; Li, M. J.; Feng, Z. C.; Chen, J.; Li, C. *J. Phys. Chem. B* **2006**, *110*, 927.
(24) Ding, X. Z.; Liu, X. H. *J. Mater. Res.* **1998**, *13*, 2556.
(25) Goldstein, A. N.; Echer, C. M.; Alivisatos, A. P. *Science* **1992**, *256*, 1425.
(26) Chen, C. C.; Herhold, A. B.; Johnson, C. S.; Alivisatos, A. P. *Science* **1997**, *276*, 398.
(27) Zhang, H. Z.; Banfield, J. F. *J. Mater. Res.* **2000**, *15*, 437.
(28) Penn, R. L.; Banfield, J. F. *Am. Mineral.* **1999**, *84*, 871.
(29) Zhang, H. Z.; Banfield, J. F. *Chem. Mater.* **2005**, *17*, 3421.
(30) Sugimoto, T.; Zhou, X. P.; Muramatsu, A. *J. Colloid Interface Sci.* **2003**, *259*, 43.
(31) Keshmiri, M.; Troczynski, T. *J. Non-Cryst. Solids* **2002**, *311*, 89.

JP808013K